



Different activation signatures in the primary sensorimotor and higher-level regions for haptic three-dimensional curved surface exploration

Jiajia Yang^{a,b,*}, Peter J. Molfese^b, Yinghua Yu^{b,c,d}, Daniel A. Handwerker^b, Gang Chen^e, Paul A. Taylor^e, Yoshimichi Ejima^a, Jinglong Wu^{f,a}, Peter A. Bandettini^{b,g}

^a Graduate School of Interdisciplinary Science and Engineering in Health Systems, Okayama University, 3-1-1 Tushima-Naka, Kita-ku, Okayama 700-8530, Japan

^b Section on Functional Imaging Methods, National Institute of Mental Health, Bethesda, MD, USA

^c Center for Information and Neural Networks, National Institute of Information and Communications Technology, Suita, Osaka, Japan

^d Graduate School of Frontier Biosciences, Osaka University, Suita, Osaka, Japan

^e Scientific and Statistical Computational Core, National Institute of Mental Health, Bethesda, MD, USA

^f Beijing Institute of Technology, Beijing, China

^g Functional MRI Core Facility, National Institute of Mental Health, Bethesda, MD, USA



ARTICLE INFO

Keywords:

Haptic object perception
Primary somatosensory cortex
Primary motor cortex
fMRI
Parametric modulation
Cortical hierarchy

ABSTRACT

Haptic object perception begins with continuous exploratory contact, and the human brain needs to accumulate sensory information continuously over time. However, it is still unclear how the primary sensorimotor cortex (PSC) interacts with these higher-level regions during haptic exploration over time. This functional magnetic resonance imaging (fMRI) study investigates time-dependent haptic object processing by examining brain activity during haptic 3D curve and roughness estimations. For this experiment, we designed sixteen haptic stimuli (4 kinds of curves \times 4 varieties of roughness) for the haptic curve and roughness estimation tasks. Twenty participants were asked to move their right index and middle fingers along the surface twice and to estimate one of the two features—roughness or curvature—depending on the task instruction. We found that the brain activity in several higher-level regions (e.g., the bilateral posterior parietal cortex) linearly increased as the number of curves increased during the haptic exploration phase. Surprisingly, we found that the contralateral PSC was parametrically modulated by the number of curves only during the late exploration phase but not during the early exploration phase. In contrast, we found no similar parametric modulation activity patterns during the haptic roughness estimation task in either the contralateral PSC or in higher-level regions. Thus, our findings suggest that haptic 3D object perception is processed across the cortical hierarchy, whereas the contralateral PSC interacts with other higher-level regions across time in a manner that is dependent upon the features of the object.

1. Introduction

In the somatosensory system, haptic perception originates through continuous exploratory contact with objects, and the human brain has to accumulate sensory information continuously across time to understand an object through touch (Klatzky and Lederman, 2011). During haptic exploration, both cutaneous and proprioceptive information are known to first arrive at the contralateral primary sensorimotor cortex (PSC) in the cerebral cortex (Pleger and Villringer, 2013; Sathian, 2016). Both nonhuman primate (NHP) (Arce-McShane et al., 2016; Umeda et al., 2019) and human neuroimaging (Huber et al., 2017) studies have demonstrated that the primary somatosensory cortex (S1) and the primary motor cortex (M1) interact with each other to shape haptic information in the early stage. After such initial sensorimotor processing in the PSC, the integrated representation of the object lo-

cal (e.g., surface roughness) and global (e.g., three-dimensional (3D) shape) features are sent to other higher-level regions for further processing (Ackerley and Kavounoudias, 2015). However, how haptic information is updated across time through the cortical hierarchy remain poorly understood.

The S1 is known to comprise four cytoarchitectonic areas (areas 3a, 3b, 1, and 2), which together are responsible for the signals from different peripheral receptors. According to the classical model of somatosensory processing from NHP studies (Delhayé et al., 2018; Mountcastle, 2005), local features such as roughness are processed by cutaneous receptors, which are conveyed to area 3b, whereas global features such as shape are handled by proprioceptive receptors, which project to area 3a. Then, neural signals from areas 3a and 3b project to areas 1 and 2, where the cutaneous information and proprioceptive information are integrated. Evidence from a recent study (Kim et al.,

* Corresponding author.

E-mail address: yang@okayama-u.ac.jp (J. Yang).

2015), however, challenges this prevalent model by demonstrating that area 3b also responds to both cutaneous and proprioceptive inputs. These findings imply that the haptic assessment of 3D objects requires the integration of cutaneous and proprioceptive inputs at all four subregions of the S1, and these initial processing steps are thought to shape the basic features of the object. Compared to the S1, the M1 (area 4) is more likely accountable for kinesthetic information processing, such as hand motion and finger positions during haptic exploration (Gurtubay-Antolin et al., 2018; Kassuba et al., 2013; Masson et al., 2016; Sathian et al., 2011).

Apart from PSCs, recent human neuroimaging studies using a variety of tasks have observed somatosensory responses in multiple higher-level regions (Sathian, 2016). Specifically, the parietal opercular cortex has been defined as the secondary somatosensory cortex (S2) (Burton, 1986), which responds to all types of sensorimotor inputs, such as object shape, size, and roughness. Furthermore, the S2 is known to bidirectionally connect to the posterior parietal cortex (PPC), to the prefrontal cortex (PFC) and to the premotor cortex (PMC) during both haptic and tactile object processing (Eickhoff et al., 2010, 2008; Rajaei et al., 2018; Sathian et al., 2011; Yang et al., 2017, 2014, 2012; Yu et al., 2018b). Although the precise contributions of each area have not yet been established, the subregions, including the anterior part of the superior parietal lobule (SPL; areas 5 and 7) and inferior parietal lobule (IPL; area 40) of the PPC, have long been associated with object local and global feature processing (Sathian, 2016). In contrast, the intraparietal sulcus (IPS) is strongly connected to the bilateral PFC and PMC, both of which have been implicated in planning complex cognitive behavior, attention, decision making, etc. (Finn et al., 2019; Hunt et al., 2018; Nee and D'Esposito, 2016; Styrkowiec et al., 2019; Tremel and Wheeler, 2015). However, it remains unclear how the PSC interacts with these higher-level regions to allow haptic information to be processed across the cortical hierarchy.

The aim of the present functional magnetic resonance imaging (fMRI) study is to investigate the cortical processing underlying haptic 3D object perception. To manipulate the local and global properties of objects, we designed a series of unique haptic stimuli sets combining local object features (roughness) and global features (3D curve), which were changed in a parametric manner. During the fMRI scan, participants explored one of sixteen curved surfaces having different roughness values (4 curve types \times 4 roughness types) in 5s and were told to estimate one of the two features depending on the task instruction (i.e., how many curves were present or how rough the surface was). This experimental design combined with the stimuli set allowed us (1) to isolate and compare regions across the whole brain relative to the surface curve and/or roughness estimation, (2) to test whether the brain regions show parametric variation based on each surface feature, and (3) to observe the brain activity across the exploration phase and to reveal the interaction between the PSC and other higher-level regions as a function of time for each surface feature.

2. Materials and methods

2.1. Participants

Twenty healthy right-handed volunteers (10 males and 10 nonpregnant females; age range 20–30 years, with a mean age of 22 ± 0.63 years) participated in the fMRI experiments. None of the participants reported a loss of tactile sensation; a history of major medical or neurological illness, such as epilepsy; significant head trauma; or a history of alcohol dependence. All of the participants gave written informed consent under the National Institutes of Health (NIH) Combined Neuroscience Institutional Review Board-approved protocol (93-M-0170, ClinicalTrials.gov identifier: NCT00001360) in accordance with the Belmont Report and US Federal Regulations that protect human participants.

2.2. Finger somatotopic mapping

One of our research goals was to investigate how haptic object estimation modulates activity in the contralateral PSC. Thus, to select precise finger regions in the contralateral PSC, we first performed somatotopic mapping for the right four fingers (index, middle, ring and pinky) using an on-off block design. The participant's right hand was extended to her/his side and comfortably supported by cushions. The experimenter stood at the entrance of the scanner bore and manually poked the participant's fingers using a plastic stick (round tip, 10 mm in diameter). The experimenter was trained, and a 4 Hz rhythmic sound train was presented to the experimenter via headphones during the on phase to control the poking frequency. During the on phase, one of the four fingers was randomly and independently poked. The participants were instructed to keep their attention on the poked finger during the on phase. The duration of each on phase (stimulation) was 17.5 s, followed by a 10.5 s or 14 s duration off phase (with the duration of the off phase randomly chosen). This on/off-phase cycle was repeated five times for each finger (a total of twenty cycles).

2.3. Haptic roughness and curve estimation task

2.3.1. Haptic stimuli

A total of 17 kinds of 3D printed haptic stimuli were used in the present study. Fig. 1a-d show the detailed parameters of the haptic stimuli. Specifically, Fig. 1a shows four kinds of global curved surfaces, which have 1, 2, 3, or 4 curves. Fig. 1b shows four kinds of local textured surfaces, consisting of tetragonal arrays of hemispheroidal raised dots with an identical distance center-to-center between adjacent dots in each row; the distances were 2, 3, 4, or 5 mm. The hemispheroidal dots had a 1 mm diameter and were raised 1.5 mm from the surface (Fig. 1c). All four types of dot patterns were printed on four different curved surfaces with a 40×100 mm² rectangular base (Fig. 1d). Fig. 1e shows an example of four stimuli with dot spacing equal to 5 mm. In total, there were sixteen haptic stimuli (4 kinds of curves \times 4 varieties of roughness) for the curve and roughness estimation tasks (Fig. 1f). Furthermore, to control the basic somatosensory input by the finger-surface contacts and hand motion, one flat surface without dots was used in the hand motion and visual control (HMVC) task (Fig. 1g). Three custom-designed, metal-free stimuli containers were used to present all stimuli in a pseudorandom order to the participants during the fMRI experiment. All stimuli shifts occurred during the pretrial interval, which was manually controlled by the experimenter standing by the MRI bore.

2.3.2. Procedures

Each participant was asked to perform four fMRI task runs that focused on roughness estimation (RE) and curve estimation (CE). Due to time limitations, three out of twenty participants performed only three task runs. First, to ensure that the participants moved their fingers at a constant speed, they performed 10–20 trials outside of the scanner. The experimenter conducted this training until he could confirm that the participant exhibited uniform motion. Each fMRI task run consisted of 48 trials (16 trials \times 3 tasks), which were pseudorandomly presented. Participants were informed that a series of surfaces would be presented. Their task was to estimate the roughness or curve of each stimulus or to move their fingers, as directed by instructions on the screen (BOLD-screen, Cambridge Research). The participants were instructed to choose a comfortable contact force and to use the same contact force across all trials during the fMRI experiment.

Roughness estimation (RE) task. For RE, roughness was not defined for the participants; instead, they were asked to use their own personal definition of haptic roughness. Specifically, the participants' estimation scale was established by presenting the smoothest and roughest stimuli before the fMRI experiment. Participants were told that these were two illustrative examples. Participants were asked to assign a whole number

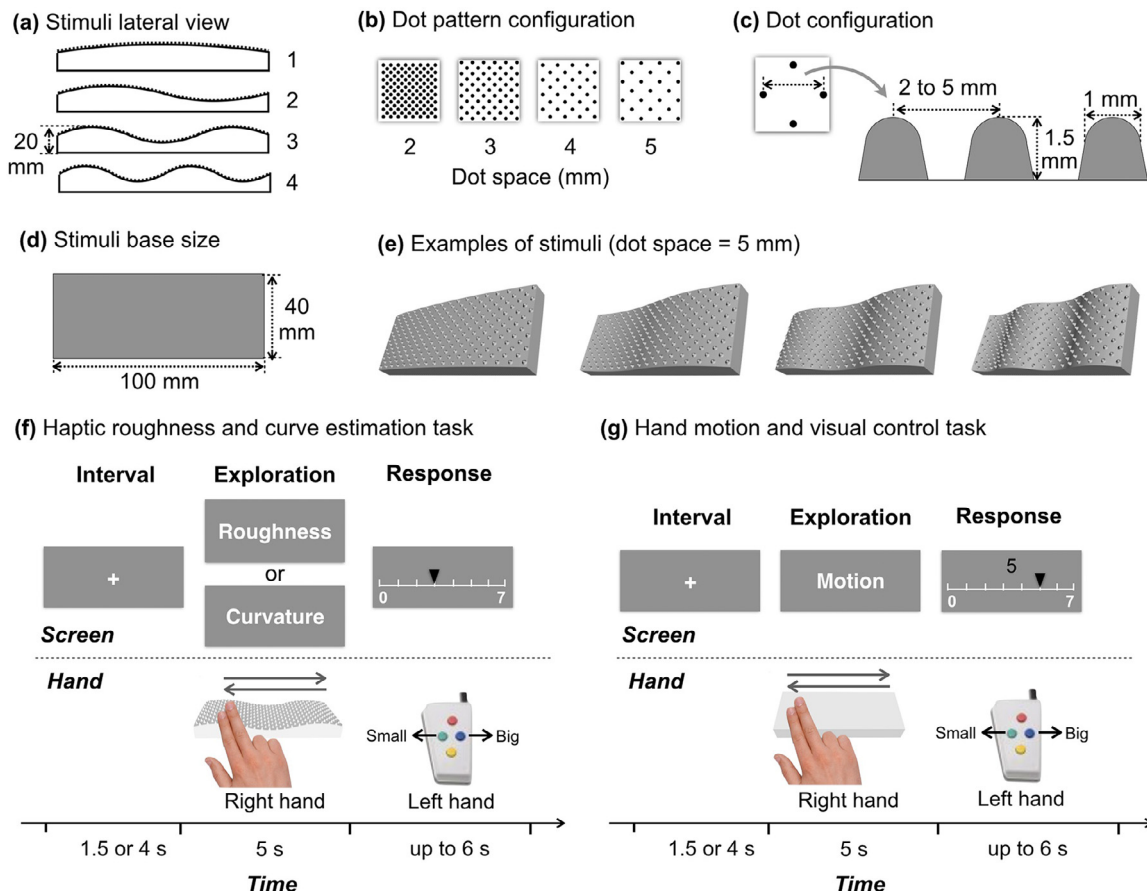


Fig. 1. Physical characteristics of the haptic stimuli and the experimental procedures. (a) Lateral view of four kinds of curved stimuli. (b) Four kinds of haptic surfaces consisting of tetragonal arrays of dots with identical dot spacing. (c) Dot heights are 1.5 mm, and dot diameters are 1 mm. (d) All four kinds of dot patterns were printed on four different surfaces with a 40 × 100 mm rectangular base. (e) Examples of stimuli with dot spacing equal to 5 mm. (f) An example trial of the roughness and curve estimation task. First, participants were asked to fixate on the visual screen. After a short interval, one of two visual instructions was presented on the screen for 5 s. During this exploration phase, participants were asked to move their right index and middle fingers right-to-left then left-to-right along the surface twice in 5 s and to perform different tasks based on the instruction. The possible instructions were as follows: “Roughness”, estimate the roughness, and “Curvature”, estimate the number of curves. Then, the participants were asked to assign a number (1 to 7) to the roughness or curves using the button box in their left hand during the response phase. (g) The HMVC task followed the same procedure, but a flat smooth surface was presented. During the exploration phase, “Motion” was presented on the screen, and the participants were asked to move their fingers right-to-left then left-to-right along a flat smooth surface twice. The participants were asked to move the triangle to the numeric location shown on the center of the screen during the response phase.

from 1 (smoothest) to 7 (roughest) that seemed appropriate to each surface. Each trial began with a short interval (1.5 s or 4 s). Subsequently, the word “Roughness” was presented during the 5 s exploration phase (see Fig. 1f). The participants were asked to move their right index and middle fingers in a right-to-left then left-to-right motion along the surface twice during the exploration phase at a constant speed. The participants were asked to ignore the curve of the stimuli and to estimate the roughness of the surface. Then, they were asked to assign a number to the roughness level using the button box in their left hand during the 6 s response phase.

Curve estimation (CE) task. For CE, the participants did not know the maximum curve number before the fMRI experiment. They were asked to estimate the number of curves and assign a whole number from 1 to 7 to each stimulus. The procedure and timing for each phase were the same as the RE task, whereas the word “Curvature” was presented during the exploration phase. The participants were asked to ignore the roughness of the surface and to estimate the number of curves.

Hand motion and visual control (HMVC) task. This task was designed to control the motor components (i.e., the right-hand exploration for the roughness/curve estimation and the left-hand rating scale selection) and the visual stimuli (i.e., the visual instructions and response scales presented on the screen). We used the same procedure as that used in

the RE and CE tasks, though a flat smooth surface was presented (see Fig. 1g). The participants were asked to just move their fingers in a right-to-left then left-to-right motion along the flat smooth surface twice. Then, the participants were asked to move the triangle to the numeric location shown on the center of the screen during the response phase.

2.4. Image acquisition

MRI scans were performed on each participant using a GE Discovery MR750 3T MRI scanner (GE Healthcare, Chicago, IL). No participant was in the scanner for longer than 120 min per session. Each scanning session consisted of acquiring the following fMRI datasets: an individual finger somatotopic mapping run that was 10 min (240 volumes) in duration, followed by three or four haptic task runs that were each 11 min in duration (265 volumes). Standard T2*-weighted echo planar imaging (EPI) sequence parameters were used to obtain the functional images and ten reverse-blip volumes with the following parameters: repetition time (TR) = 2500 ms, echo time (TE) = 30 ms, phase encoding = A to P, flip angle = 75°, matrix = 77 × 77, axial slices = 42, in-plane field of view = 186 × 186 mm², in-plane resolution = 2.58 × 2.58 mm², and slice thickness = 3.0 mm (whole-brain coverage). After the fMRI acquisition, a T1-weighted magnetization prepared rapid gradient echo

(MPRAGE) high-resolution anatomical volume was obtained with the following parameters: voxel size = $1.0 \times 1.0 \times 1.0 \text{ mm}^3$, TR = 7040 ms, TE = 3480 ms, matrix = $256 \times 256 \times 172$, and duration = 5 min.

2.5. Behavioral data analysis

The RE and CE estimates (scale values) and response times of each participant were collected with open-source application PsychoPy software v1.85.0 (Peirce et al., 2019). The R programming language (R Core Team, 2013) was used for additional statistical analyses.

2.6. fMRI data analyses

fMRI data were analyzed using “*afni_proc.py*” with the AFNI/SUMA (version = 18.1.08) software package (<http://afni.nimh.nih.gov/>) (Cox, 1996; Saad et al., 2006). Cortical surfaces for each participant were created using FreeSurfer (Version 6.0) (<http://surfer.nmr.mgh.harvard.edu/>) (Fischl, 2012) by running the “recon-all” command for each T1-weighted anatomical image and converting the results from the standard NIFTI/GIFTI format to AFNI “@SUMA_Make_Spec_FS”.

2.6.1. Individual participants: preprocessing and modeling

The full “*afni_proc.py*” command used to generate the processing stream and quality control is provided in the *Supplementary material*. We briefly describe the implemented processing blocks and options used here. Before statistical analysis, the first two volumes of each run were removed, and slice-timing correction was then performed to adjust for differences in slice-acquisition times. Then, we applied blip up/down nonlinear alignment to all EPI images and then aligned all images to participants’ own anatomical image (Glen et al., 2020). Motion correction with rigid-body (three translation and three rotation) alignment was performed, and volumes with Euclidean norm (enorm) of the rigid-body motion parameters greater than 0.3 mm were censored. EPIs were mapped to the surface domain and blurred to a smoothness of 6 mm full width at half maximum (FWHM) on the surface. Finally, each node’s time series was scaled to have a mean of 100, so that time series fluctuations would correspond to interpretable units of local blood-oxygen level dependent (BOLD) percent signal changes (Chen et al., 2017).

Within the “*afni_proc.py*” command, a general linear model (GLM) was also fitted to the fMRI data for each participant. The BOLD signal was modeled for the finger somatotopic mapping run, and all haptic RE and CE task runs with a block function were convolved with the canonical hemodynamic response function (HRF) using the AFNI “3dDeconvolve” command. Assuming a first-order autoregressive model, the serial autocorrelation was estimated from the pooled active nodes with the restricted maximum likelihood procedure. The motion-related artifacts were minimized via the incorporation of six parameters (three translations and three rotations) from the rigid-body realignment stage into each model. The estimates were evaluated using linear contrasts of finger data relative to baseline in each participant or in each task. Furthermore, aside from the visual data confirmation, the output of the AFNI “@ss_review_basic” for each participant’s processing was used for quality control; this output comprised the max motion, temporal signal-to-noise ratio (tSNR), smoothing values, counts of outliers, etc.

Then, we obtained the subbrick images (section 2.6.2) to localize the mean specific PSC subregions, (section 2.6.3) observe the whole-brain activity pattern during the CE and RE tasks, (section 2.6.4) and observe the brain regions parametrically modulated by CE and RE tasks. Finally, we also performed (section 2.6.5) a time series analysis to observe the time series data from the contralateral PSC and other higher-level regions.

2.6.2. Group analysis: localize specific PSC subregions for the index and middle fingers

First, a one-sample t-test was used to confirm the activation of each finger (index, middle, ring and pinky) from the finger somatotopic map-

ping run. The height threshold was set at $p < 0.002$ ($t_{19} > 3.6$, two-sided testing) (Chen et al., 2019; Eklund et al., 2016), and the threshold for the spatial extent test was set at $p < 0.05$. This finger somatotopic mapping run was designed to select precise finger regions in the contralateral PSC, which were used to investigate how haptic object estimation modulates activity in these regions. Since all participants were asked to touch the stimuli using their right index and middle fingers during the CE and RE tasks, we classified activations for only index and middle fingers around the postcentral gyrus (poCG) into four subregions (areas 3a, 3b, 1, and 2) within the S1 and M1 (area 4).

2.6.3. Group analysis: average activity modulation by CE and RE tasks

First, analysis of variance (ANOVA) was used to confirm the whole-brain activation of each task (RE, CE, and HMVC). We then evaluated the contrast of the mean of the RE task with the mean of the HMVC task (RE – HMVC) and the contrast of the mean of the CE task with the mean of the HMVC task (CE – HMVC). We then evaluated the contrasts of (CE – HMVC) – (RE – HMVC) and (RE – HMVC) – (CE – HMVC) to identify brain regions affected by the haptic curve and roughness estimations. The height threshold was set at $p < 0.002$ ($t_{19} > 3.6$, two-sided testing), and the threshold for the spatial extent test was set at $p < 0.05$.

2.6.4. Group analysis: parametric main effects of CE and RE tasks

To locate any regions that showed a parametric response to CEs and REs, we next performed whole-brain group analysis with parametric regressors (Chen et al., 2014). The linearity across the four levels of each task (roughness or curve) was assessed through post hoc inferences in the 2×2 within-subject ANOVA model using “3dMVM” in AFNI. Specifically, a set of weights of -3, -1, 1 and 3 (normalized to have a zero-mean) were assigned to the four levels of each task to infer the linearity. These four weights corresponded to the first-order orthogonal polynomials evaluated at four equally spaced data points. Both the height threshold and spatial extent thresholds were set the same as above.

2.6.5. Time series analysis

To examine the parametric main effects in the contralateral PSC and higher-level regions across the exploration phase, we further estimated the activation of these regions at each time point. We defined contralateral areas 4, 3a, 3b, 1, and 2 from the independent somatotopic mapping run, and the higher-level regions were defined from the CE of specific regions (i.e., the surviving regions from the (CE – HMVC) – (RE – HMVC) contrast). Then, we extracted all the functional time series signals at these specified regions for all participants from the scaled EPIs in the surface space. Finally, these signals were convolved with a TENT function of the “3dDeconvolve” in AFNI to estimate the response amplitude (% signal change) for each region to each task trial. Linear mixed-effects model analysis was performed using the “lme4” package in R (Bates et al., 2015) to evaluate the brain activation time series of each region. Here, we set time factors at two levels, which corresponded to the early and late exploration phases. The stimuli factors were set at four levels, corresponding to stimuli curves or roughness. If there was a significant interaction between the time and stimuli level, a post hoc test was conducted for the simple effect of the stimuli; otherwise, the main effect of the stimuli was examined. These p values were Bonferroni-corrected.

3. Results

3.1. Behavioral performance

Eighteen of twenty participants (for technical reasons, behavioral data for two participants were lost) were included in the behavioral data analysis. As shown in Fig. 2, linear regression analysis (blue lines in Fig. 2) revealed that the scale values of both roughness [$r^2 = 0.744$, $p < 0.001$] and curve [$r^2 = 0.875$, $p < 0.001$] estimation were significantly increased depending on the stimuli level. Furthermore, we found

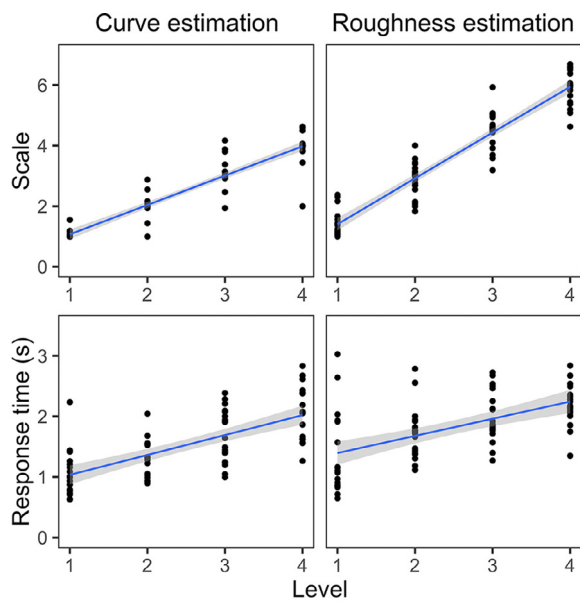


Fig. 2. Behavioral performance of curve and roughness estimation tasks. Black dots represent the average scale or response time of each participant. The blue lines represent the linear regression line. The gray background represents the 95% confidence interval.

that participants evenly assigned RE values from 1 to 7 for RE, whereas they mostly assigned CE values from 1 to 5 for CE. This difference reflected that the participants were able to scale the stimuli dependent on different physical features. In addition, we also performed linear regres-

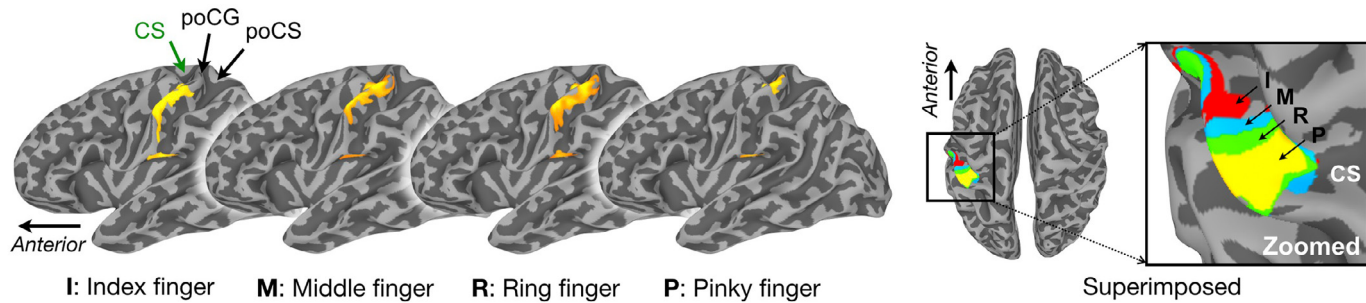
sion analysis on the mean response times for all tasks (relative to the offset of the exploration phase). We found that the response times were significantly increased dependent on the stimuli level in both roughness [$r^2 = 0.302, p < 0.001$] and curve [$r^2 = 0.465, p < 0.001$] estimation tasks. Furthermore, a two-way (two tasks \times four stimuli levels) repeated measures ANOVA of the mean response time also revealed significant main effects of the stimuli level [$F_{3, 51} = 43.58; p < 0.001$] and task [$F_{1, 17} = 14.38; p = 0.001$] without interaction [$F_{3, 51} = 1.49; p = 0.228$]. On one hand, the response time main effect of the stimuli level reflected a larger scale value the more the button was pressed. On the other hand, the response time main effect of the task revealed that the participants provided a CE faster than an RE. In the present study, since the participants were asked to assign a number to the stimulus during the response phase rather than respond as quickly as possible, the difference in response time had a negligible contribution to brain activation.

3.2. fMRI results

3.2.1. Somatotopic maps

For all participants, finger activation maps were observed within the central sulcus (CS), poCG and poCS contralateral to the stimulated fingers. Fig. 3a shows the averaged ($n = 20$) activation maps for the right four fingers. Consistent with previous studies (Besle et al., 2013; Martuzzi et al., 2014; Stringer et al., 2014), we found that the four fingers were sequentially organized in a somatotopic manner in the posterior bank of the CS, whereas this finger response selectivity was less prominent in the poCG. Then, we defined index and middle finger corresponding sensorimotor subregions relative to the anatomical landmarks on the CS, poCG, and poCS (Fig. 3b). Specifically, areas 3a and 3b are known to be located along the posterior bank of the CS, area 1 is on

(a) Somatotopic maps of four fingers



(b) Location of sensorimotor subregions for index and middle fingers

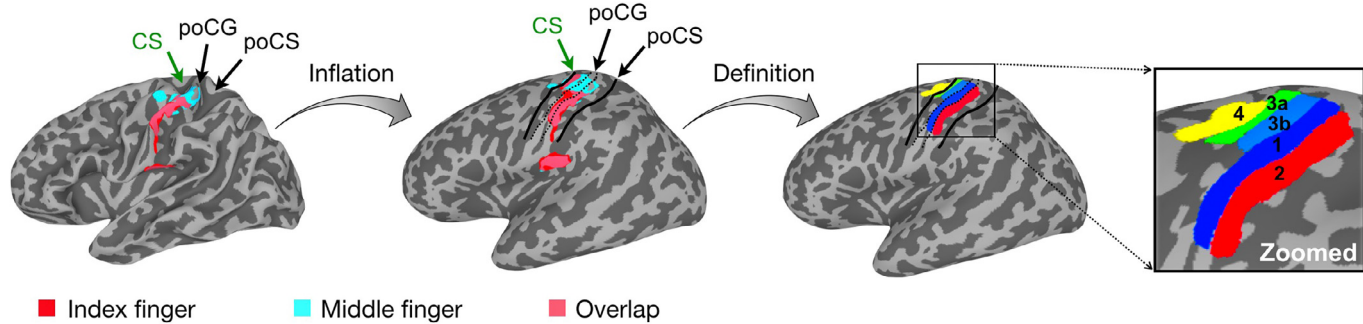


Fig. 3. Somatotopic maps and location of sensorimotor subregions. (a) Illustration of the averaged activation maps of the right four fingers. For all participants, finger maps were observed within the CS, poCG and poCS contralateral to the stimulated fingers. Furthermore, we found that the four fingers were sequentially organized (from the index finger to the pinky finger) in a somatotopic manner in the posterior bank of the CS, whereas this finger response selectivity was less prominent in the poCG. (b) Illustration of the location of the sensorimotor subregions. Based on the landmarks, we generated the masks of areas 4, 3a, 3b, 1 and 2 according to the averaged activations of the index and middle fingers. CS, central sulcus; poCG, postcentral gyrus; poCS, postcentral sulcus.

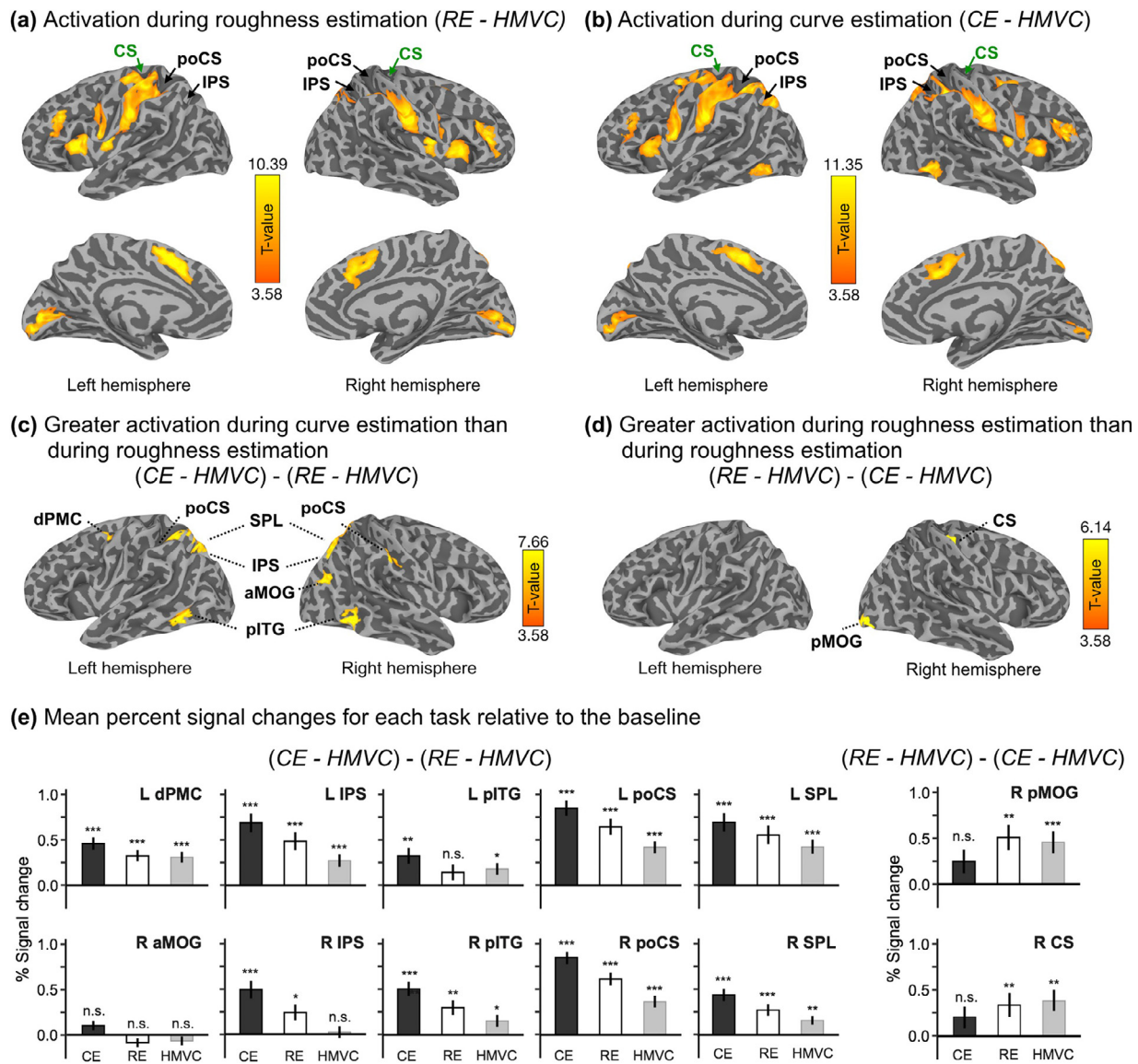


Fig. 4. Mean ($n = 20$) brain activation of roughness estimation (RE) and curve estimation (CE) rendered on cortical surfaces using SUMA. (a) Brain regions exhibiting greater activation during the RE task than during the HMVC task. (b) Brain regions exhibiting greater activation during the CE task than during the HMVC task. (c) Brain regions for the (CE - HMVC) - (RE - HMVC) contrast. (d) Brain regions for the (RE - HMVC) - (CE - HMVC) contrast. (e) These bar graphs represent the mean % signal changes in each region of interest (ROI) for each task ($n = 20$). The error bars indicate the standard error of the mean (SEM). CS, central sulcus; poCS, postcentral sulcus; IPS, intraparietal sulcus; dPMC, dorsal premotor cortex; SPL, superior parietal lobule; pITG, posterior part of the inferior temporal gyrus; aMOG, anterior middle occipital gyrus; pMOG, posterior middle occipital gyrus. Asterisks represent the statistical significance of the one-sample t-test. *: $p < 0.05$, **: $p < 0.01$, ***: $p < 0.001$, n.s.: not significant.

the crown of the poCG, and area 2 resides on the posterior bank of the poCG. Furthermore, hand area 4 is known to be located on the hand knob of the preCG.

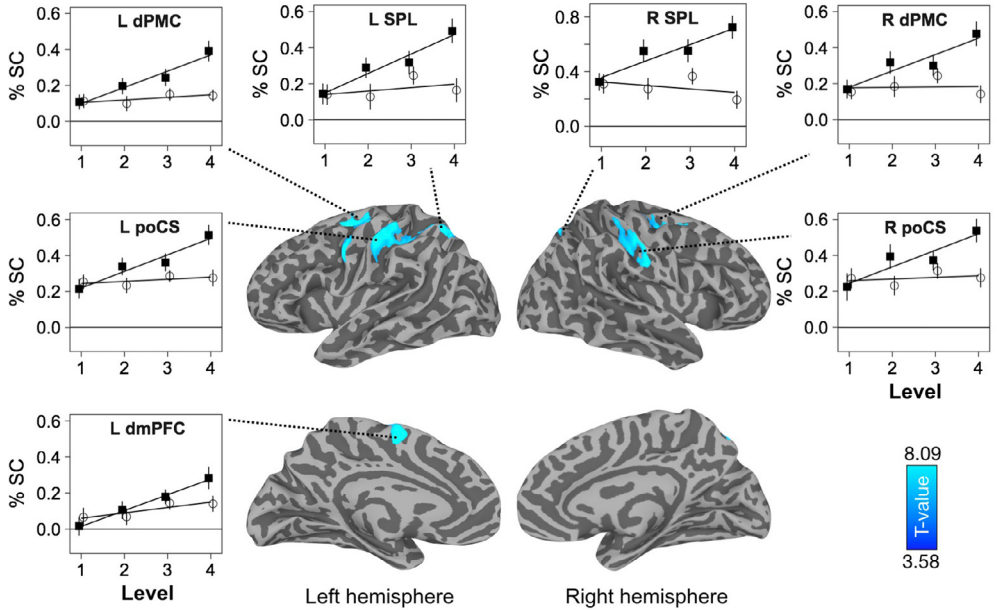
3.2.2. Whole-brain neural activity for roughness and curve estimations

Initially, we confirmed that both the RE and CE tasks (relative to the HMVC task) activated a widespread set of brain regions, including the contralateral preCG, CS and poCG (Fig. 4a, b). In addition, we also found significant activations in the bilateral ventrolateral prefrontal cortex (vlPFC), dorsal and ventral premotor cortex (dPMC and vPMC, respectively), insular cortex, parietal operculum (PO), dorsomedial prefrontal cortex (dmPFC), calcarine sulcus, right poCS, right poCG, right IPS, and right SPL. Moreover, we also found that the CE task, but not the RE task, significantly activated the bilateral posterior part of the inferior temporal gyrus (pITG), left IPS, and left SPL.

3.2.3. Whole-brain neural activity for curve estimation vs. roughness estimation and vice versa

As shown in Fig. 4c, the regions including the bilateral poCS, IPS, SPL and pITG, as well as the left dPMC and right anterior middle occipital gyrus (aMOG), were activated more strongly in the CE task than in the RE task. In contrast, the (RE - HMVC) - (CE - HMVC) result only showed stronger activation in the right posterior middle occipital gyrus (pMOG) and CS (Fig. 4d). Furthermore, to visualize the task-related signal changes in these regions, we extracted the mean activity signal (% signal change) of each task relative to the rest intervals (Fig. 4e). For regions that showed greater activation in the CE task than in the RE task, we found that the CE task elicited positive signals relative to the rest intervals for nine of ten regions (i.e., except for the right aMOG). In contrast, the regions (i.e., the right pMOG and CS) that showed greater activation during the RE task than during the CE task were also acti-

(a) Brain regions showing parametric main effects of curve estimation.



(b) Brain regions showing parametric main effects of roughness estimation.

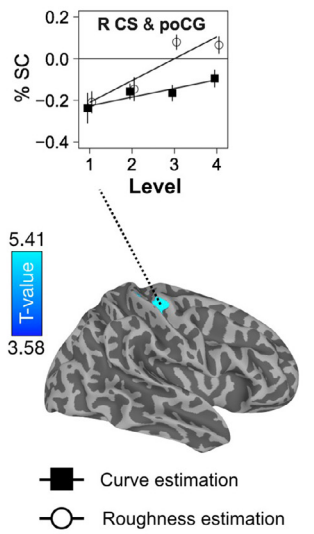


Fig. 5. Brain regions showing parametric main effects of (a) curve estimation and (b) roughness estimation. These plots represented the mean activation in each ROI for each task per stimulus level across participants ($n = 20$). For the CE task, levels 1 to 4 represent the number of curves. For the RE task, levels 1 to 4 represent the surface roughness. The error bars indicate the standard error of the mean (SEM). CS, central sulcus; poCG, postcentral gyrus; poCS, postcentral sulcus; SPL, superior parietal lobule; dPMC, dorsal premotor cortex; dmPFC, dorsomedial prefrontal cortex.

vated by the HMVC task, which may not contribute to the roughness estimation processing.

3.2.4. Brain regions showing parametric main effects of roughness and curve estimation

Fig. 5a shows that the activation of these brain regions linearly increased as the number of curves increased. These regions include the bilateral dPMC, poCS, SPL, and left dmPFC. Then, we extracted the mean activity signal of each of these seven clusters for CE and RE tasks to confirm the linear relationship between the stimuli level and brain activation. As shown in the plots of Fig. 5a, the brain activations of these regions showed linear increases relative to the CE level (black squares) but not for the RE level (outlined circles). Compared to the results of the CE task, we uniquely identified that the right CS that extended to the poCG (CS & poCG) was parametrically modulated by the RE task (Fig. 5b).

3.2.5. Time series analysis results for roughness and curve estimations

The averaged fMRI time series data in five contralateral PSC subregions and seven higher-level regions are shown in Figs. 6 and 7. Note that since three of the ten regions (i.e., left and right pITG, right aMOG) from the (CE - HMVC) - (RE - HMVC) contrast did not demonstrate parametric effects for all time points, we only illustrated the other seven regions here. In Figs. 6 and 7, the zero point of the horizontal axis represents the onset of stimulus exploration for each experimental trial, which continued for 5 s. To reveal the detailed brain activation during the exploration phase, we estimated the peak time points for the early and late phases by convolving the canonical HRF with a 2.5 s boxcar function. We noted that the early phase activation peak appeared at approximately 6.2 s, and the late phase appeared at approximately 8.6 s. Since the TR interval was 2.5 s, the data points of 7.5 s and 10 s reflected the peak activation of the early and late parts of the stimuli exploration phase separately. We found that contralateral PSC subregions showed significantly different activation patterns from those found in higher-level regions (Fig. 6a, b). Specifically, for contralateral PSC subregions (Fig. 6a), we only found parametric modulation during the CE task in

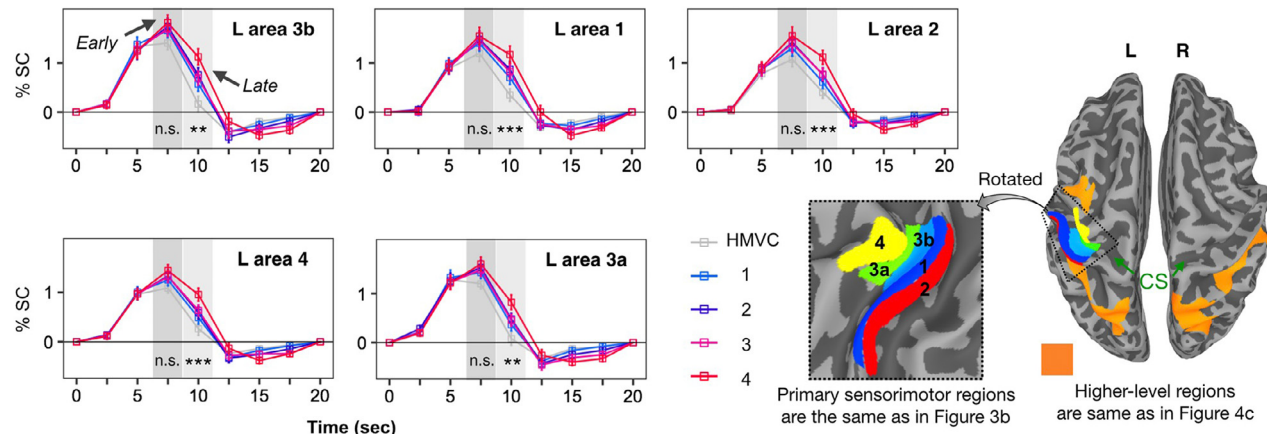
the late phase but not in the early phase. In contrast, in the higher-level regions, for example, in the activation of the left SPL (Fig. 6b), we found a linear increase relative to the CE level in both the early and late phases. In contrast, as shown in Fig. 7a, b, we did not find similar time-dependent activation profiles in either the contralateral PSC subregions or higher-level regions for the RE task.

4. Discussion

In the present study, we investigated brain activity during haptic curve and roughness estimation using a parametric fMRI experiment. Our results extend beyond the previous findings (Mueller et al., 2019; Sathian et al., 2011; Stilla and Sathian, 2008) by revealing brain regions that show parametric variation that is dependent on the curve ratings (Fig. 5a). Furthermore, our experimental design enabled us to observe brain activity across the exploration phase (i.e., early and late phase) in the contralateral PSCs and other higher-level regions during the haptic curve and roughness estimation. In particular, we found that only activation of the higher-level regions showed linear increases relative to the number of curves through the exploration phase (Fig. 6b), whereas we found that the contralateral PSC (Fig. 6a) was parametrically modulated by the number of curves only during the late exploration phase. In contrast, these time-dependent brain activity features in the same sort of regions did not appear during the haptic roughness estimation (Fig. 7a, b). Together, our findings suggest that haptic 3D object perception is processed across the cortical hierarchy, whereas the contralateral PSC interacts with other higher-level regions across time in a manner that is dependent upon object features.

First, we confirmed that both haptic CE and RE tasks produced very similar brain activity maps relative to the HMVC task (Fig. 4a, b). One straightforward interpretation of such results is that participants were asked to use the same approach to explore the same stimuli in both CE and RE tasks while estimating one of each surface feature following the instruction. This approach has the advantage of keeping the stimuli constant across tasks, and both CEs and REs would be determined by

(a) Averaged activation profiles in the contralateral primary sensorimotor regions



(b) Averaged activation profiles in higher-level regions

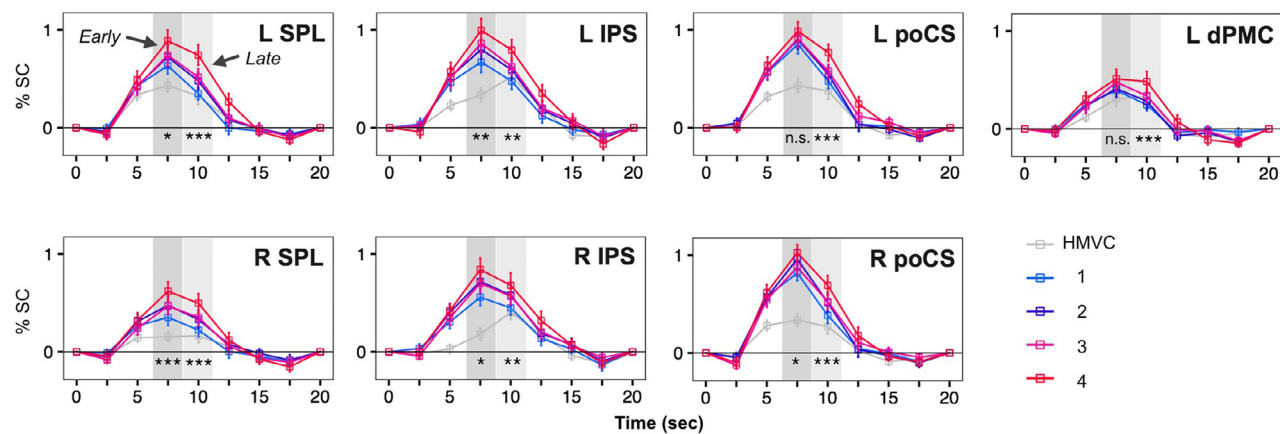


Fig. 6. Activation profiles at each time point during haptic curve estimation. (a) Averaged activation profiles in the contralateral sensorimotor regions. (b) Averaged activation profiles in higher-level regions. The error bars indicate the standard error of the mean (SEM). The darker gray square in each plot represents the activation peak for the early exploration phase, and the light gray square represents the activation peak for the late exploration phase. Asterisks represent the statistical significance of the post hoc test. *: $p < 0.05$, **: $p < 0.01$, ***: $p < 0.001$, n.s.: not significant.

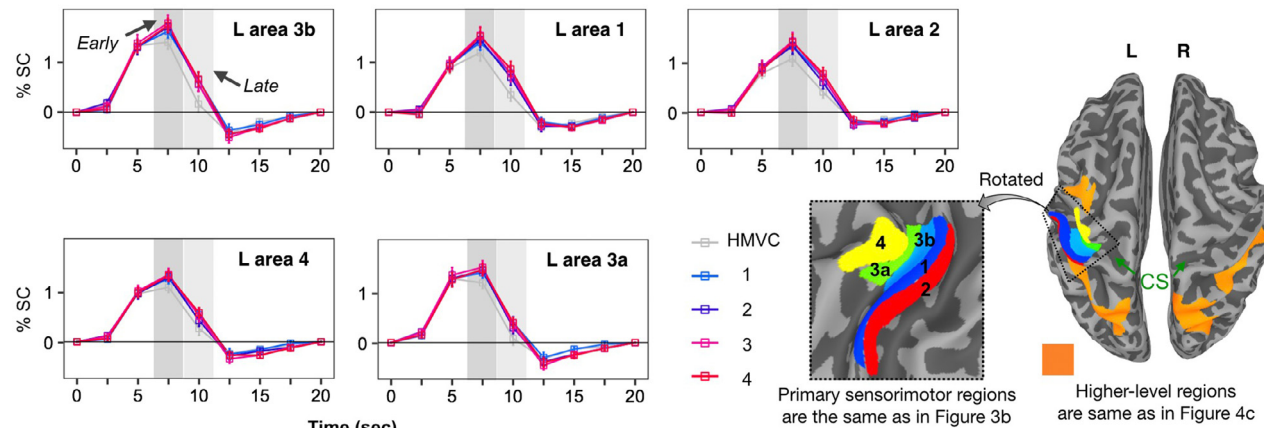
similar amounts of cutaneous and proprioceptive inputs. Furthermore, since we found that all participants can scale both curve and roughness properly in a few seconds (Fig. 2), we can assume that attentional demands were comparable between CE and RE tasks. Therefore, the direct comparison between CE and RE tasks can reveal the regions activated more strongly for each surface feature. For instance, we confirmed that haptic CE activated a higher-level region (Fig. 4c) compared to that activated during haptic RE, which has been well discussed in previous studies (Mueller et al., 2019; Sathian et al., 2011; Stillia and Sathian, 2008). These regions were thought to contribute to the extraction of the 3D geometric information (curves) from objects or other higher-level processing such as visual imagery (Deshpande et al., 2010; Kassuba et al., 2013; Lacey et al., 2010). However, the point to note here is that these regions not only contributed to CE but also contributed to RE. The evidence shown in Fig. 4e supported this point by observing significant activation in eight of ten regions during the RE task. In contrast, even though we found two regions (Fig. 4d) in the (RE - HMVC) - (CE - HMVC) contrast, the HMVC task also activated these regions at the same level (Fig. 4e) rather than specific for roughness and curve estimations.

Interestingly, our results highlighted that haptic CE parametrically modulated the activations depending on the exploration phase within the contralateral PSC (i.e., areas 4, 3a, 3b, 1 and 2) and several higher-level regions. Specifically, whole-brain parametric analysis revealed that the activations of several higher-level regions, including the bilateral

poCS, SPL, dPMC, and left dmPFC (Fig. 5a), were uniquely and linearly increased with increasing number of curves. Nonetheless, looking beyond the fMRI adaptation effects (Barron et al., 2016; Krekelberg et al., 2006; Larsson and Smith, 2012), time series analysis also revealed significant curve parametric modulation in all contralateral PSC subregions at the late exploration phase but not the early exploration phase (Fig. 6a). Such findings suggest the possibility that the contralateral PSC and these higher-level regions interacted differently across the haptic exploration phase for CE.

Human sensory processing is considered to typically occur within a hierarchical framework, consisting of a series of discrete stages from the primary sensory cortex to the whole brain. In the somatosensory system, sensorimotor information is projected initially to the contralateral PSC, encoding basic perceptual dimensions, such as edge, roughness and hand motion (Pleger and Villringer, 2013; Sathian, 2016). Then, following higher stages beyond the contralateral PSC, the second-order sensory cortex, such as areas 1 and 2, is known to have bilateral receptive fields (Iwamura, 1998) that are sensitive to hand movement direction and object shape (Sathian, 2016). Aside from these somatosensory areas, the caudal part of the SPL (i.e., area 7) also appears to be involved in the higher-order processing of sensorimotor information. Furthermore, area 7 is known to functionally connect with the bilateral SPL, dPMC, and dmPFC (the putative human supplementary motor area), and this network is thought to function in integrative sensory,

(a) Averaged activation profiles in the contralateral primary sensorimotor regions



(b) Averaged activation profiles in higher-level regions

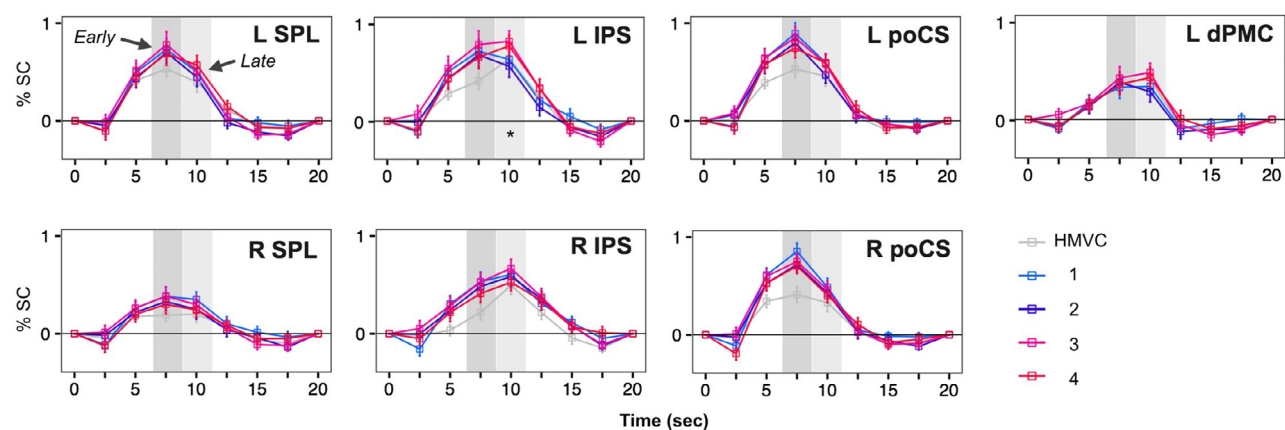


Fig. 7. Activation profiles at each time point during haptic roughness estimation. (a) Averaged activation profiles in contralateral sensorimotor regions. (b) Averaged activation profiles in higher-level regions. The error bars indicate the standard error of the mean (SEM). The darker gray square in each plot represents the activation peak for the early exploration phase, and the light gray square represents the activation peak for the late exploration phase. The asterisk represents the statistical significance of the post hoc test for $p < 0.05$, and no other time points reached significance.

motor and cognitive functions (Freedman and Ibos, 2018; Nelson et al., 2010). Therefore, the parametric modulation in these higher-level regions through the exploration phase may represent higher-order functions such as curve reconstruction and finger motion control during exploration.

In contrast, this strict bottom-up formation cannot adequately explain why we only found parametric modulation in the contralateral PSC during the late exploration phase but not during the early exploration phase. One possible interpretation of our finding is related to bidirectional hierarchy models such as predictive coding theoretical frameworks (de Lange et al., 2018; Friston, 2010), in which the lower sensory cortex receives not only bottom-up input but also top-down feedback (Yu et al., 2019b, 2019a, 2018a). Thus, our findings suggest that prior experience with the curved surface may provide top-down feedback to modulate the contralateral PSC in a parametric manner during the late exploration phase. In the present study, the participants were asked to explore each surface twice during the exploration phase. It is reasonable to assume that the participants would detect the number of curves during the first exploration (roughly during the early phase), and the second exploration (roughly during the late phase) was more likely to confirm the answer. Thus, one important insight from these data is that the physical properties, such as the number of curves, might not be parametrically encoded in the contralateral PSC, while top-down feedback modulation may occur in the contralateral PSC.

For RE, we did not find parametric modulation in the contralateral PSC and these higher-level regions during either the early or late exploration phase (Fig. 7a, b). Even we found that the participants assigned different scales for the CE and RE tasks, the difference in scales has a negligible contribution to this result. Because the scales were only used to confirm whether the participants could estimate each feature of the stimuli, and the parametric main effects were examined for each feature of the stimuli separately. From the behavioral perspective, this result may reflect that the participants are more likely to assign a number to the roughness at the end of the exploration since roughness has an abstractive definition. Thus, they may not easily remember it as a number at the early exploration phase, as was the case in the CE task. From the brain function perspective, this finding may reflect the different coding and processing between roughness and curve in the human brain. Both the findings, as shown in Fig. 4c of the present study and in previous neuroimaging studies (Kassuba et al., 2013; Stilla and Sathian, 2008), may support this assumption. For example, we found that the activations of the bilateral SPL, IPS, and pITG are significantly stronger for CE than those of RE, and these regions demonstrated a tendency to be more specialized for visual object processing (Kassuba et al., 2013; Stilla and Sathian, 2008). In contrast, regions such as the S2 are more sensitive to the haptic perception of surface roughness processing (Stilla and Sathian, 2008). Despite this, we cannot exclude the contribution of other factors, such as the basic properties of the roughness

stimulus. For example, previous behavior studies (Dépeault et al., 2009; Eck et al., 2013) have used dot spacings ranging from 1.5 to 8.5 mm, whereas in the present study, we used dot spacings ranging from 1 to 5 mm, which limited us to observing the parametric modulation. Much more work is necessary to resolve these issues.

5. Conclusion

In summary, consistent with previous studies, we found that haptic curve and roughness processing share many cortical regions. Beyond these previous findings, we found that CE parametrically modulated activation in the contralateral PSC and bilateral poCS, SPL, dPMC, and left dmPFC but not RE. Furthermore, we found remarkable differences in exploration phase-dependent brain activation between the contralateral PSC and higher-level regions related to haptic CE. This finding may represent the nature of time-dependent interactions across the sensory information cortical hierarchy that shape our behavior.

Data and code availability

Raw data for the empirical results presented of this study are available in [OpenNeuro: <https://openneuro.org>] with the accession number [“ds003466”]. The AFNI codes used to generate the data processing stream and quality control is provided in the Supplementary material.

Author contributions

J.Y., P.M., Y.Y., and P.B. designed and performed the fMRI experiments. D.H., Y.E., and J.W. contributed to the conception and design. J.Y., P.M., G.C., and P.T. analyzed the fMRI data. J.Y., P.M., Y.Y., and PB wrote the paper. All authors discussed and commented on the manuscript.

Declaration of Competing Interest

All authors declare that they have no other competing interests.

Finding

This work was supported by JSPS KAKENHI Grant Numbers JP20K07722, JP18H01411 and Japan-U.S. Science and Technology Co-operation Program (Brain Research).

Acknowledgments

We thank Vinai Roopchansingh and John Andrew Derbyshire for the fMRI sequence used here. We thank Natasha Topolski for support of human volunteer scanning. We thank the NIH machine shop for help with 3d-printing the stimuli and device. The research was conducted as part of the NIMH Intramural Research Program (#ZIA-MH002783).

Supplementary materials

Supplementary material associated with this article can be found, in the online version, at doi:[10.1016/j.neuroimage.2021.117754](https://doi.org/10.1016/j.neuroimage.2021.117754).

References

- Ackerley, R., Kavounoudias, A., 2015. The role of tactile afference in shaping motor behaviour and implications for prosthetic innovation. *Neuropsychologia* 79, 192–205. doi:[10.1016/j.neuropsychologia.2015.06.024](https://doi.org/10.1016/j.neuropsychologia.2015.06.024).
- Arce-McShane, F.I., Ross, C.F., Takahashi, K., Sessle, B.J., Hatsopoulos, N.G., 2016. Primary motor and sensory cortical areas communicate via spatiotemporally coordinated networks at multiple frequencies. *Proc. Natl. Acad. Sci. U. S. A.* 113, 5083–5088. doi:[10.1073/pnas.1600788113](https://doi.org/10.1073/pnas.1600788113).
- Barron, H.C., Garvert, M.M., Behrens, T.E.J., 2016. Repetition suppression: a means to index neural representations using BOLD? *Philos. Trans. R. Soc. B Biol. Sci.* 371. doi:[10.1098/rstb.2015.0355](https://doi.org/10.1098/rstb.2015.0355).
- Bates, D., Mächler, M., Bolker, B., Walker, S., 2015. Fitting linear mixed-effects models using lme4. *J. Stat. Softw.* 67. doi:[10.18637/jss.v067.i01](https://doi.org/10.18637/jss.v067.i01).
- Besle, J., Sánchez-Panchuelo, R.M., Bowtell, R., Francis, S., Schluppeck, D., 2013. Single-subject fMRI mapping at 7 T of the representation of fingertips in S1: a comparison of event-related and phase-encoding designs. *J. Neurophysiol.* 109, 2293–2305. doi:[10.1152/jn.00499.2012](https://doi.org/10.1152/jn.00499.2012).
- Burton, H., 1986. Second somatosensory cortex and related areas. In: Jones, E.G., Peters, A. (Eds.), *Sensory-Motor Areas and Aspects of Cortical Connectivity*. Springer, US, Boston, MA, pp. 31–98. doi:[10.1007/978-1-4613-2149-1_2](https://doi.org/10.1007/978-1-4613-2149-1_2).
- Chen, G., Adleman, N.E., Saad, Z.S., Leibnauft, E., Cox, R.W., 2014. Applications of multivariate modeling to neuroimaging group analysis: a comprehensive alternative to univariate general linear model. *Neuroimage* 99, 571–588. doi:[10.1016/j.neuroimage.2014.06.027](https://doi.org/10.1016/j.neuroimage.2014.06.027).
- Chen, G., Cox, R.W., Glen, D.R., Rajendra, J.K., Reynolds, R.C., Taylor, P.A., 2019. A tail of two sides: Artificially doubled false positive rates in neuroimaging due to the sidedness choice with t-tests. *Hum. Brain Mapp.* 40, 1037–1043. doi:[10.1002/hbm.24399](https://doi.org/10.1002/hbm.24399).
- Chen, G., Taylor, P.A., Cox, R.W., 2017. Is the statistic value all we should care about in neuroimaging? *Neuroimage* 147, 952–959. doi:[10.1016/j.neuroimage.2016.09.066](https://doi.org/10.1016/j.neuroimage.2016.09.066).
- Cox, R.W., 1996. AFNI: software for analysis and visualization of functional magnetic resonance neuroimages. *Comput. Biomed. Res.* 29, 162–173. doi:[10.1006/cbmr.1996.0014](https://doi.org/10.1006/cbmr.1996.0014).
- de Lange, F.P., Heilbron, M., Kok, P., 2018. How do expectations shape perception? *Trends Cogn. Sci.* 22, 764–779. doi:[10.1016/j.tics.2018.06.002](https://doi.org/10.1016/j.tics.2018.06.002).
- Delhayé, B.P., Long, K.H., Bensmaia, S.J., 2018. Neural basis of touch and proprioception in primate cortex. *Compr. Physiol.* 8, 1575–1602. doi:[10.1002/cphy.c170033](https://doi.org/10.1002/cphy.c170033).
- Dépeault, A., Metfah, E.M., Chapman, C.E., 2009. Tactile perception of roughness: raised-dot spacing, density and disposition. *Exp. Brain Res.* 197, 235–244. doi:[10.1007/s00221-009-1907-1](https://doi.org/10.1007/s00221-009-1907-1).
- Deshpande, G., Hu, X., Lacey, S., Still, R., Sathian, K., 2010. Object familiarity modulates effective connectivity during haptic shape perception. *Neuroimage* 49, 1991–2000. doi:[10.1016/j.neuroimage.2009.08.052](https://doi.org/10.1016/j.neuroimage.2009.08.052).
- Eck, J., Kaas, A.L., Mulders, J.L.J., Goebel, R., 2013. Roughness perception of unfamiliar dot pattern textures. *Acta Psychol. (Amst.)* 143, 20–34. doi:[10.1016/j.actpsy.2013.02.002](https://doi.org/10.1016/j.actpsy.2013.02.002).
- Eickhoff, S.B., Grefkes, C., Fink, G.R., Zilles, K., 2008. Functional lateralization of face, hand, and trunk representation in anatomically defined human somatosensory areas. *Cereb. Cortex* 18, 2820–2830. doi:[10.1093/cercor/bhn039](https://doi.org/10.1093/cercor/bhn039).
- Eickhoff, S.B., Jbabdi, S., Caspers, S., Laird, A.R., Fox, P.T., Zilles, K., Behrens, T.E., 2010. Anatomical and functional connectivity of cytoarchitectonic areas within the human parietal operculum. *J Neurosci* 30, 6409–6421. doi:[10.1523/jneurosci.5664-09.2010](https://doi.org/10.1523/jneurosci.5664-09.2010).
- Eklund, A., Nichols, T.E., Knutsson, H., 2016. Cluster failure: why fMRI inferences for spatial extent have inflated false-positive rates. *Proc. Natl. Acad. Sci. U. S. A.* 113, E4929. doi:[10.1073/pnas.1612033113](https://doi.org/10.1073/pnas.1612033113).
- Finn, E.S., Huber, L., Jangraw, D.C., Molfese, P.J., Bandettini, P.A., 2019. Layer-dependent activity in human prefrontal cortex during working memory. *Nat. Neurosci.* 22, 1687–1695. doi:[10.1038/s41593-019-0487-z](https://doi.org/10.1038/s41593-019-0487-z).
- Fischl, B., 2012. FreeSurfer. *Neuroimage* 62, 774–781. doi:[10.1016/j.neuroimage.2012.01.021](https://doi.org/10.1016/j.neuroimage.2012.01.021).
- Freedman, D.J., Ibos, G., 2018. An integrative framework for sensory, motor, and cognitive functions of the posterior parietal cortex. *Neuron* 97, 1219–1234. doi:[10.1016/j.neuron.2018.01.044](https://doi.org/10.1016/j.neuron.2018.01.044).
- Friston, K., 2010. The free-energy principle: a unified brain theory? *Nat. Rev. Neurosci.* 11, 127–138. doi:[10.1038/nrn2787](https://doi.org/10.1038/nrn2787).
- Glen, D.R., Taylor, P.A., Buchsbaum, B.R., Cox, R.W., Reynolds, R.C., 2020. Beware (Surprisingly Common) left-right flips in your MRI Data: an efficient and robust method to check MRI dataset consistency using AFNI. *Front. Neuroinform.* 14, 1–7. doi:[10.3389/fninf.2020.00018](https://doi.org/10.3389/fninf.2020.00018).
- Gurtubay-Antolin, A., León-Cabrera, P., Rodríguez-Fornells, A., 2018. Neural evidences of hierarchical cognitive control during haptic processing: an fMRI study. *eneuro* 5. doi:[10.1523/ENEURO.0295-18.2018](https://doi.org/10.1523/ENEURO.0295-18.2018), e0295-18, 2018.
- Huber, L., Handwerker, D.A., Jangraw, D.C., Chen, G., Hall, A., Stüber, C., Gonzalez-Castillo, J., Ivanov, D., Marrett, S., Guidi, M., Goense, J., Poser, B.A., Bandettini, P.A., 2017. High-resolution CBV-fMRI allows mapping of laminar activity and connectivity of cortical input and output in human M1. *Neuron* 96, 1253–1263. doi:[10.1016/j.neuron.2017.11.005](https://doi.org/10.1016/j.neuron.2017.11.005).
- Hunt, L.T., Malalasekera, W.M.N., de Berker, A.O., Miranda, B., Farmer, S.F., Behrens, T.E.J., Kennerley, S.W., 2018. Triple dissociation of attention and decision computations across prefrontal cortex. *Nat. Neurosci.* 21, 1471–1481. doi:[10.1038/s41593-018-0239-5](https://doi.org/10.1038/s41593-018-0239-5).
- Iwamura, Y., 1998. Hierarchical somatosensory processing. *Curr. Opin. Neurobiol.* 8, 522–528. doi:[10.1016/S0959-4388\(98\)80041-X](https://doi.org/10.1016/S0959-4388(98)80041-X).
- Kassab, T., Klinge, C., Hölig, C., Röder, B., Siebner, H.R., 2013. Vision holds a greater share in visuo-haptic object recognition than touch. *Neuroimage* 65, 59–68. doi:[10.1016/j.neuroimage.2012.09.054](https://doi.org/10.1016/j.neuroimage.2012.09.054).
- Kim, S.S., Gomez-ramirez, M., Thakur, P.H., Hsiao, S.S., 2015. Multimodal interactions between proprioceptive and cutaneous signals in primary somatosensory cortex. *Neuron* 86, 555–566. doi:[10.1016/j.neuron.2015.03.020](https://doi.org/10.1016/j.neuron.2015.03.020).
- Klatzky, R.L., Lederman, S.J., 2011. Haptic object perception: spatial dimensionality and relation to vision. *Philos. Trans. R. Soc. B Biol. Sci.* 366, 3097–3105. doi:[10.1098/rstb.2011.0153](https://doi.org/10.1098/rstb.2011.0153).
- Krekelberg, B., Boynton, G.M., van Wezel, R.J.A., 2006. Adaptation: from single cells to BOLD signals. *Trends Neurosci.* 29, 250–256. doi:[10.1016/j.tins.2006.02.008](https://doi.org/10.1016/j.tins.2006.02.008).
- Lacey, S., Flueckiger, P., Still, R., Lava, M., Sathian, K., 2010. Object familiarity modulates the relationship between visual object imagery and haptic shape perception. *Neuroimage* 49, 1977–1990. doi:[10.1016/j.neuroimage.2009.10.081](https://doi.org/10.1016/j.neuroimage.2009.10.081).

- Larsson, J., Smith, A.T., 2012. FMRI repetition suppression: neuronal adaptation or stimulus expectation? *Cereb. Cortex* 22, 567–576. doi:[10.1093/cercor/bhr119](https://doi.org/10.1093/cercor/bhr119).
- Martuzzi, R., van der Zwaag, W., Farthouat, J., Gruetter, R., Blanke, O., 2014. Human finger somatotopy in areas 3b, 1, and 2: A 7T fMRI study using a natural stimulus. *Hum. Brain Mapp.* 35, 213–226. doi:[10.1002/hbm.22172](https://doi.org/10.1002/hbm.22172).
- Masson, H.L., Bulthé, J., Beeck, H.P., Op De, Wallraven, C., 2016. Visual and haptic shape processing in the human brain: unisensory processing, multisensory convergence, and top-down influences. *Cereb. Cortex* 26, 3402–3412. doi:[10.1093/cercor/bhv170](https://doi.org/10.1093/cercor/bhv170).
- Mountcastle, V.B., 2005. The Sensory Hand: Neural Mechanisms of Somatic Sensation. Harvard University Press doi:[10.1086/509471](https://doi.org/10.1086/509471).
- Mueller, S., de Haas, B., Metzger, A., Drewing, K., Fiehler, K., 2019. Neural correlates of top-down modulation of haptic shape versus roughness perception. *Hum. Brain Mapp.* 40, 5172–5184. doi:[10.1002/hbm.24764](https://doi.org/10.1002/hbm.24764).
- Nee, D.E., D'Esposito, M., 2016. The hierarchical organization of the lateral prefrontal cortex. *Elife* 5, 1–26. doi:[10.7554/elife.12112](https://doi.org/10.7554/elife.12112).
- Nelson, S.M., Cohen, A.L., Power, J.D., Wig, G.S., Miezin, F.M., Wheeler, M.E., Venanova, K., Donaldson, D.I., Phillips, J.S., Schlaggar, B.L., Petersen, S.E., 2010. A parcellation scheme for human left lateral parietal cortex. *Neuron* 67, 156–170. doi:[10.1016/j.neuron.2010.05.025](https://doi.org/10.1016/j.neuron.2010.05.025).
- Peirce, J., Gray, J.R., Simpson, S., MacAskill, M., Höchenberger, R., Sogo, H., Kastman, E., Lindeløv, J.K., 2019. PsychoPy2: Experiments in behavior made easy. *Behav. Res. Methods* 3, 1–9. doi:[10.3758/s13428-018-01193-y](https://doi.org/10.3758/s13428-018-01193-y).
- Pleger, B., Villringer, A., 2013. The human somatosensory system: from perception to decision making. *Prog. Neurobiol.* 103, 76–97. doi:[10.1016/j.pneurobio.2012.10.002](https://doi.org/10.1016/j.pneurobio.2012.10.002).
- R Core Team, 2013. R: A language and environment for statistical computing. R Foundation for Statistical Computing doi:[10.1007/978-3-540-74686-7](https://doi.org/10.1007/978-3-540-74686-7).
- Rajaei, N., Aoki, N., Takahashi, H.K., Miyaoka, T., Kochiyama, T., Ohka, M., Sadato, N., Kitada, R., 2018. Brain networks underlying conscious tactile perception of textures as revealed using the velvet hand illusion. *Hum. Brain Mapp.* 39, 4787–4801. doi:[10.1002/hbm.24323](https://doi.org/10.1002/hbm.24323).
- Saad, Z.S., Chen, G., Reynolds, R.C., Christidis, P.P., Hammett, K.R., Bellgowan, P.S.F., Cox, R.W., 2006. Functional imaging analysis contest (FIAC) analysis according to AFNI and SUMA. *Hum. Brain Mapp.* 27, 417–424. doi:[10.1002/hbm.20247](https://doi.org/10.1002/hbm.20247).
- Sathian, K., 2016. Analysis of haptic information in the cerebral cortex. *J. Neurophysiol.* 116, 1795–1806. doi:[10.1152/jn.00546.2015](https://doi.org/10.1152/jn.00546.2015).
- Sathian, K., Lacey, S., Stillia, R., Gibson, G.O., Deshpande, G., Hu, X., LaConte, S., Glielmi, C., 2011. Dual pathways for haptic and visual perception of spatial and texture information. *Neuroimage* 57, 462–475. doi:[10.1016/j.neuroimage.2011.05.001](https://doi.org/10.1016/j.neuroimage.2011.05.001).
- Stillia, R., Sathian, K., 2008. Selective visuo-haptic processing of shape and texture. *Hum. Brain Mapp.* 29, 1123–1138. doi:[10.1002/hbm.20456](https://doi.org/10.1002/hbm.20456).
- Stringer, E.A., Qiao, P.G., Friedman, R.M., Holroyd, L., Newton, A.T., Gore, J.C., Chen, L.M., 2014. Distinct fine-scale fMRI activation patterns of contra- and ipsilateral somatosensory areas 3b and 1 in humans. *Hum. Brain Mapp.* 35, 4841–4857. doi:[10.1002/hbm.22517](https://doi.org/10.1002/hbm.22517).
- Styrkowicz, P.P., Nowik, A.M., Króliczak, G., 2019. The neural underpinnings of haptically guided functional grasping of tools: an fMRI study. *Neuroimage* 194, 149–162. doi:[10.1016/j.neuroimage.2019.03.043](https://doi.org/10.1016/j.neuroimage.2019.03.043).
- Tremel, J.J., Wheeler, M.E., 2015. Content-specific evidence accumulation in inferior temporal cortex during perceptual decision-making. *Neuroimage* 109, 35–49. doi:[10.1016/j.neuroimage.2014.12.072](https://doi.org/10.1016/j.neuroimage.2014.12.072).
- Umeda, T., Isa, T., Nishimura, Y., 2019. The somatosensory cortex receives information about motor output. *Sci. Adv.* 5, eaaw5388. doi:[10.1126/sciadv.aaw5388](https://doi.org/10.1126/sciadv.aaw5388).
- Yang, J., Han, H., Chui, D., Shen, Y., Wu, J., 2012. Prominent activation of the intraparietal and somatosensory areas during angle discrimination by intra-active touch. *Hum. Brain Mapp.* 33, 2957–2970. doi:[10.1002/hbm.21419](https://doi.org/10.1002/hbm.21419).
- Yang, J., Kitada, R., Kochiyama, T., Yu, Y., Makita, K., Araki, Y., Wu, J., Sadato, N., 2017. Brain networks involved in tactile speed classification of moving dot patterns: the effects of speed and dot periodicity. *Sci. Rep.* 7, 1–13. doi:[10.1038/srep40931](https://doi.org/10.1038/srep40931).
- Yang, J., Yu, Y., Kunita, A., Huang, Q., Wu, J., Sawamoto, N., Fukuyama, H., 2014. Tactile priming modulates the activation of the fronto-parietal circuit during tactile angle match and non-match processing: an fMRI study. *Front. Hum. Neurosci.* 8, 1–8. doi:[10.3389/fnhum.2014.00926](https://doi.org/10.3389/fnhum.2014.00926).
- Yu, Y., Huber, L., Chai, Y., Jangraw, D.C., Khojandi, A., Yang, J., Bandettini, P.A., 2019a. Increased activity in superficial and deep layers of human S1 for temporal prediction error. In: *Proc. Intl. Soc. Mag. Reson. Med.*, p. 27.
- Yu, Y., Huber, L., Jangraw, D.C., Molfese, P.J., Hall, A., Handwerker, D.A., Yang, J., Bandettini, P.A., 2018a. Depth-dependent functional mapping of mental prediction in human somatosensory cortex. In: *Proc. Intl. Soc. Mag. Reson. Med. 26. International Society for Magnetic Resonance in Medicine, Paris, France*, p. 393 16–21 June.
- Yu, Y., Huber, L., Yang, J., Jangraw, D.C., Handwerker, D.A., Molfese, P., Chen, G., Ejima, Y., Wu, J., Bandettini, P.A., 2019b. Layer-specific activation of sensory input and predictive feedback in the human primary somatosensory cortex. *Sci. Adv.* 5, eaav9053. doi:[10.1126/sciadv.aav9053](https://doi.org/10.1126/sciadv.aav9053).
- Yu, Y., Yang, J., Ejima, Y., Fukuyama, H., Wu, J., 2018b. Asymmetric functional connectivity of the contra- and ipsilateral secondary somatosensory cortex during tactile object recognition. *Front. Hum. Neurosci.* 11 (662), 1–7. doi:[10.3389/fnhum.2017.00662](https://doi.org/10.3389/fnhum.2017.00662).